Research Article
doi.org/10.1002/batt.202200279

Chemistry Europe
European Chemical Societies Publishing

www.batteries-supercaps.org

Understanding the Capacity Fade in Polyacrylonitrile Binder-based $LiNi_{0.5}Mn_{1.5}O_4$ Cells**

Alma Mathew,[a] Casimir Misiewicz,[a] Matthew J. Lacey,[b] Satu Kristiina Heiskanen,[c] Jonas Mindemark,[a] Erik Berg,[a] Reza Younesi,[a] and Daniel Brandell*[a]

Binders are electrochemically inactive components that have a crucial impact in battery ageing although being present in only small amounts, typically 1–3% w/w in commercial products. The electrochemical performance of a battery can be tailored via these inactive materials by optimizing the electrode integrity and surface chemistry. Polyacrylonitrile (PAN) for $LiNi_{0.5}Mn_{1.5}O_4$ (LNMO) half-cells is here investigated as a binder material to enable a stable electrode-electrolyte interface. Despite being previously described in literature as an oxidatively stable polymer, it is shown that PAN degrades and develops resistive layers within the LNMO cathode. We demonstrate continuous internal resistance increase in LNMO-based cells during battery operation using intermittent current interruption (ICI) technique. Through a combination of on-line electrochemical mass spectrometry (OEMS) and X-ray photoelectron spectroscopy (XPS) characterization techniques, the degradation products can be identified as solid on the LNMO electrode surface, and no excessive gas formation seen. The increased resistance and parasitic processes are correlated to side-reactions of the PAN, possibly intramolecular cyclization, which can be identified as the main cause of the comparatively fast capacity fade.

Introduction

Extensive research is being made in the field of lithium-ion batteries (LIBs) correlated to the increasing demand for electric vehicles. $LiNi_{0.5}Mn_{1.5}O_4$ (LNMO) is in this context a highly promising LIB cathode material owing to its high energy density, roughly on par with $Li(Ni_xMn_yCo_z)O_2$ (NMC) cells, high power density, but perhaps primarily due to it being completely free from the environmentally, socially, and economically problematic element cobalt, which otherwise is standard in most LIB cathodes. Moreover, LNMO is compared to other chemistries Mn-rich, which is considerably cheaper than Ni.[1] While having a moderate specific capacity of 147 $mAh\,g^{-1}$, LNMO has a high operating voltage at around 4.7 V (vs. Li/Li^+) corresponding to the Ni^{2+}/Ni^{4+} active redox couple. The 3-D diffusion channels present in the intrinsic spinel structure of LNMO allows fast lithiation and delithiation kinetics in the crystal, which contribute to excellent rate capability and render the material suitable for high power applications.[2] However, the oxidative decomposition of electrolyte at higher voltages, dissolution of transition metals (both Mn^{2+} and Ni^{2+} ions) during cycling and severe capacity fade at elevated temperatures are major challenges for commercialization of this material.[2,3] Despite intense research efforts, it is still not clear to what extent these stability issues are related to the surface and bulk properties of the electrode.[1,4]

Understanding the electrochemistry of LNMO and modifying this cathode material to mitigate transition metal dissolution, reduce the capacity fade and thereby improve the performance of this LIB system will be key for future success. Extensive studies therefore exist on the synthesis conditions of the active material,[5] dependence on the size and particle morphology,[6,7] elemental doping,[8] various surface coating strategies using inorganic and organic materials[9–11] and also significant research in the direction of alternate electrolyte compositions and additives.[2,12] As LNMO operates at high voltages, beyond the electrochemical stability window of conventional electrolytes, the oxidation of electrolyte is presently one main limitation for LNMO cells. This highlights the importance of the surface chemistry in LNMO-based cells. It has been suggested that reducing the direct contact of the active particle with the electrolyte by surface coating or formation of a stable passivation layer on the surface can lead to a lower capacity fade.[10,13]

Moreover, several investigations have demonstrated that tailoring the binder system or modifying the active material particles with a polymer coating generate significant changes in the surface chemistry, thereby also resulting in improve-

[a] A. Mathew, C. Misiewicz, Dr. J. Mindemark, Prof. E. Berg, Dr. R. Younesi, Prof. D. Brandell
Department of Chemistry – Ångström Laboratory
Uppsala University
Box 538, 75121 Uppsala, Sweden
E-mail: daniel.brandell@kemi.uu.se
[b] Dr. M. J. Lacey
Scania CV AB
15187 Södertälje, Sweden
[c] Dr. S. K. Heiskanen
Volkswagen AG
38436 Wolfsburg, Germany

[**] A previous version of this manuscript has been deposited on a preprint server (https://doi.org/10.26434/chemrxiv-2022-jrcft).

Supporting information for this article is available on the WWW under https://doi.org/10.1002/batt.202200279

ments in the electrochemical performance.[14] At the battery anode side, it is well-demonstrated that appropriate selection of the binder has enabled improved performance via protection of the surface, so a similarly well-chosen binder could also confer a protective effect at a cathode material.[15] Many polymers, however, can display significant electrochemical decomposition at the high operating voltages required for LNMO cells.[16] It is therefore important to ensure that when choosing a polymer either as a binder or as a coating for LNMO, it should be oxidatively stable at higher voltages, or that its decomposition products protect from further decomposition of the electrolyte, analogous to the solid electrolyte interphase (SEI) at the anode.

Polynitriles contain the strongly electron-withdrawing and polar nitrile group (–C≡N). The high polarity renders it potentially advantageous as a binder, as it can form comparatively strong bonds with both the active particles and the current collector.[17] Moreover, polynitriles possess a combination of Li ion conductivity and good oxidation stability, which is important for cells operating at higher voltages.[18,19] Nitrile solvents for electrolytes have been successfully explored at high voltages, but their high intrinsic viscosity and the reductive decomposition of these electrolyte at the carbonaceous anode are major drawbacks.[20] A potential advantage of using similar materials as cathode binders is that the relative immobility of the polymer means that any such issues of reduction at the anode may be avoided.

The most used polynitrile in LIB research is poly(acrylonitrile) (PAN), and its employment with LNMO electrodes has been previously reported. Panero and co-workers for example exploited PAN-based composite gel polymer electrolytes in $LiPF_6$-propylene carbonate solution for LNMO cells, and suggested that the anodic stability window stretched up to 5.5 V vs. Li/Li^+.[21] Lin et al. used cyclized PAN (c-PAN) as a surface coating for LNMO particles by a simple heat treatment method, and observed an improvement in the cycling of LNMO cells both at room temperature and at 55 °C compared to the pristine LNMO cells.[22] Tanaka and co-workers studied the role of an acrylonitrile-grafted poly(vinyl alcohol) (PAN-g-PVA) copolymer as a binder for LNMO cathodes and showed that it enhances the cyclability of half-cells as compared to a PVdF (poly(vinylidene difluoride))-based cell.[23] It was argued that these improvements are due to the higher adhesive strength of PVA and oxidation resistance of PAN.

Although the binder amount contributes only to a small portion of the total electrode composition, it plays a large role in maintaining the electrochemical stability and performance. Physical properties such as conductivity, mechanical strength, dispersion, thermal and chemical stability, etc., are crucial for choosing the right binder material for a LIB electrode.[24] Jeschull et al. has shown that binder swelling negatively impacts the electrode degradation of graphite electrodes and should be prevented.[14] Conventional LIBs primarily use PVdF as binder due to its chemical inertness, thermal stability and good adhesion properties with the active material and the current collector. Copolymers of vinylidene difluoride and hexafluropropylene (HFP) are also commonly used, as PVdF-HFP copolymers offer high mechanical strength, higher solubility, and better flexibility.[25] In this present work, we investigate the functionality of nitrile-based polymers as binders, using PAN for a range of binder concentrations. While PAN displays less anodic stability than PVdF-HFP, the strongly electron-withdrawing nature and high polarity renders it an ion-coordinating polymer, create stronger surface interactions, and an improved distribution in the electrode. A uniform coating on the cathode surface can be expected from strong interactions between the polynitriles with the active particles, which thereby can reduce electrolyte oxidation. Herein, we have focused on the interaction of the binder, specifically PAN, with the cathode material and the impact of binder concentration on the cycling stability to better elucidate the role of the binder for LNMO electrode degradation.

Results and Discussion

Surface chemistry

The surface morphology of the pristine electrodes was determined using SEM. Figure 1 shows the EDX mapping images and SEM micrographs in the insets of the 2.5PAN and 2.5PVdF-HFP electrodes, respectively. The EDX mapping images were obtained at a 5 kV accelerating voltage. The colour code to understand the EDX maps is provided at the bottom left corner of each image. The electrode with the spherical LNMO particles displays an excellent distribution of the carbon black conductive additive and the PAN binder, as observed in Figure 1(a and c), rather than forming non-uniform polymer binder-carbon islands as observed with the PVdF-HFP binder in Figure 1(b and d). The active LNMO particles are largely uncovered by the carbon black and the PVdF-HFP binder in the case of the 2.5PVdF-HFP binder, implying that LNMO has direct contact with the electrolyte during galvanostatic cycling. The strong polarity of the polymer likely accounts for the homogeneous surface coverage of the PAN-based electrode.[17]

Electrochemistry

The electrochemical tests were carried out using both PAN and PVdF-HFP binder-based LNMO electrodes at different binder concentrations. The electrochemical tests were performed in the range of 3.5–5.0 V vs. Li/Li^+ at room temperature. Following three formation cycles at C/10, further cycling was done at C/5 rate. Figure 2(a) shows that increasing PAN binder content in the electrode leads to an increased capacity fade in the LNMO half-cells. The cell with 2.5PAN binder in the LNMO electrode showed the highest capacity retention after 95 cycles with a discharge capacity of 134 $mAh\,g^{-1}$. The cell with the highest PAN binder concentration, i.e., 20 wt.%, exhibited a rapid fade in discharge capacity, showing only 64 $mAh\,g^{-1}$ at the end of 95 cycles. Figure 2(b) shows the Coulombic efficiency of these PAN based cells, which follows the same trend as the discharge capacity. The galvanostatic cycling results with PAN binder

Research Article
doi.org/10.1002/batt.202200279
Chemistry Europe
European Chemical Societies Publishing

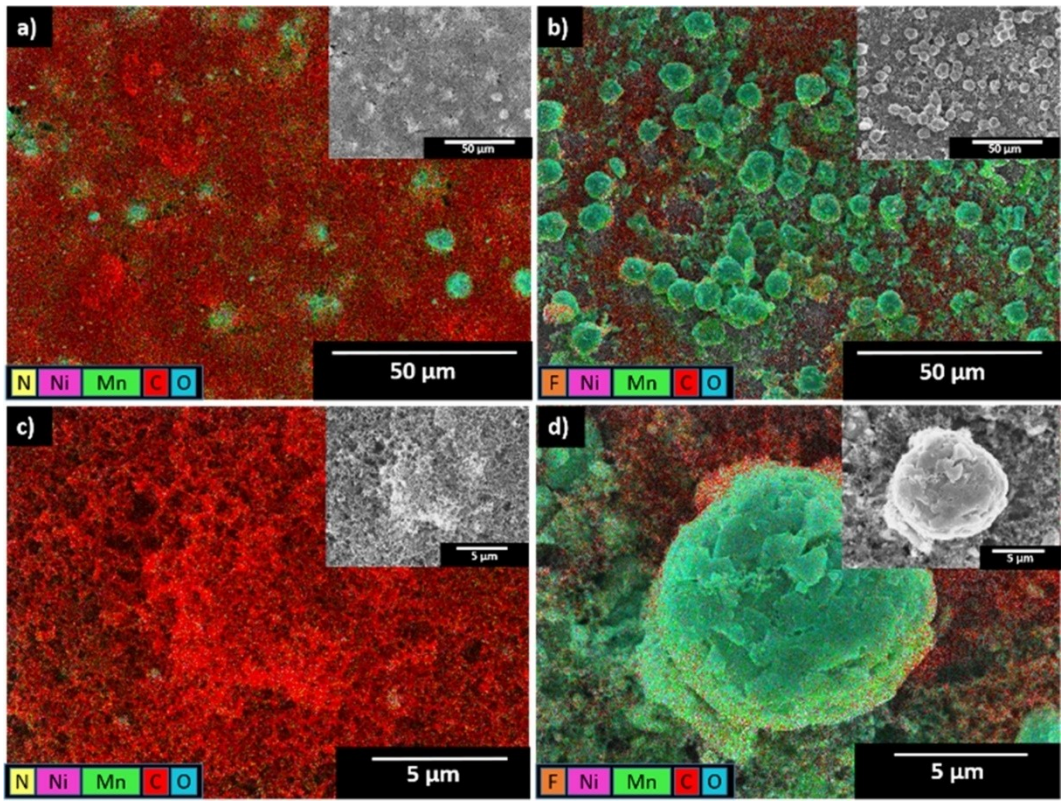

Figure 1. EDX mapping of pristine electrodes: a) and c) with 2.5PAN, and b) and d) with 2.5PVdF-HFP binder. The corresponding SEM micrographs are provided in the insets.

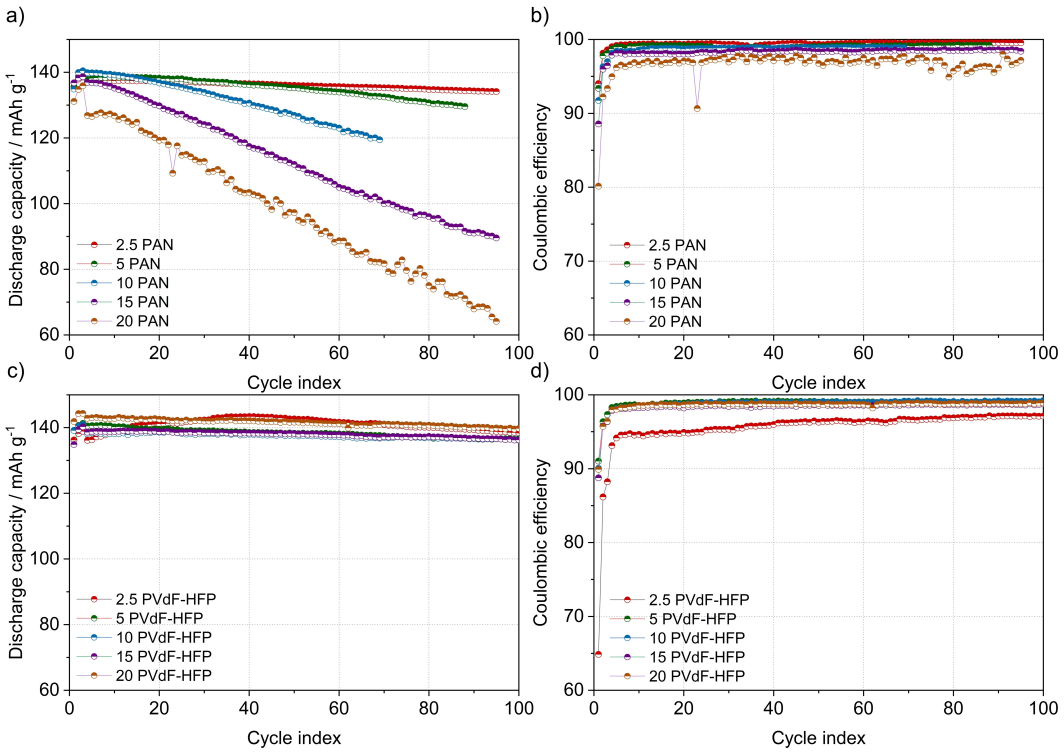

Figure 2. Cycling performance of LNMO half cells at C/10 for 3 cycles and C/5 for further cycles. a) discharge capacity vs. cycle number using different concentrations (2.5, 5, 10, 15 and 20 wt.%) of PAN binder b) Coulombic efficiencies of the corresponding PAN-based cells c) discharge capacity vs. cycle number for LNMO half-cells using different concentrations (2.5, 5, 10, 15, 20 wt.%) of PVdF-HFP binder, d) Coulombic efficiencies of the corresponding PVdF-HFP-based cells. Figure S1 shows data that has been zoomed in.

Research Article
doi.org/10.1002/batt.202200279

were compared with the standard PVdF-HFP binder at different binder concentrations. The discharge capacity vs. cycle number plot in Figure 2(c) shows that using PVdF-HFP as an LNMO electrode binder does not follow the same trend as using PAN. When compared to PAN, PVdF-HFP generally shows a higher capacity retention, as observed in Figure 2(c). The strong trend of faster capacity fade with increasing binder content in PAN-containing cells on the other hand indicates that a degradation reaction is taking place, with higher quantities of degradation occurring in cells with higher PAN concentrations, and that these side-reactions affects capacity degradation. These side reactions in PAN-containing cells are most likely caused by the binder, being the only change in electrode composition, and this in turn affects the carbon black-binder network negatively, resulting in the loss of electrode integrity, poor electronic conductivity and thereby capacity fade.

Intermittent current interruption and electrochemical impedance spectroscopy

In order to understand the simultaneous resistance changes in the PAN-based LNMO cell, the intermittent current interruption (ICI) method was utilized. The 2.5PAN and 10PAN LNMO cell were chosen for the ICI measurements and the results could be straight-forwardly compared with the corresponding PVdF-HFP cell. Figure 3 shows an overview of the 10PAN ICI results. ICI data for the 2.5PAN cell and a comparison with 2.5PVdF-HFP is provided in Figure S2. The voltage profiles (E) of charge and discharge cycles of the 1st, 10th, 50th and 100th cycles as a function of capacity are presented together with the corresponding internal resistance (R) curves. The ICI measurements were carried out at a rate of C/10, and the results with PAN and PVdF-HFP binders in LNMO electrodes are shown in corresponding colors. During the 1st charge, R, which is the total resistance contribution from electronic, ionic and charge-transfer resistances[26] shows a drop at the end of the charge and then gradually increases during the discharge step. The resistance during charge and discharge for 10PAN and 10PVdF does not appear to differ significantly during the 10th cycle. When compared to 10PVdF-HFP, 10PAN has a higher resistance in the 100th cycle, which is reflected in the large hysteresis seen in the charge-discharge curves. The 3rd, 4th and 5th row in Figure 3 indicates the coulombic efficiency, discharge capacity and median resistance with cycle number up to 100 cycles, respectively, for the same cells. It can be observed that the rapid decrease in discharge capacity with cycle number is correlated with the increase in median resistance in the cell with PAN as binder. The increasing resistance with cycle number suggests PAN degradation and resistance build-up in the cell. The ionic and electronic resistances in the electrode are directly associated to electrochemical processes such as ionic transport and electronic conduction in the electrode, and the resistance build-up in the cell is likely strongly correlated to capacity fading in these cells.[27] The fact that the PAN cells do not attain the full theoretical capacity, as demonstrated by the voltage profiles in cycles 50 and 100, implies that high

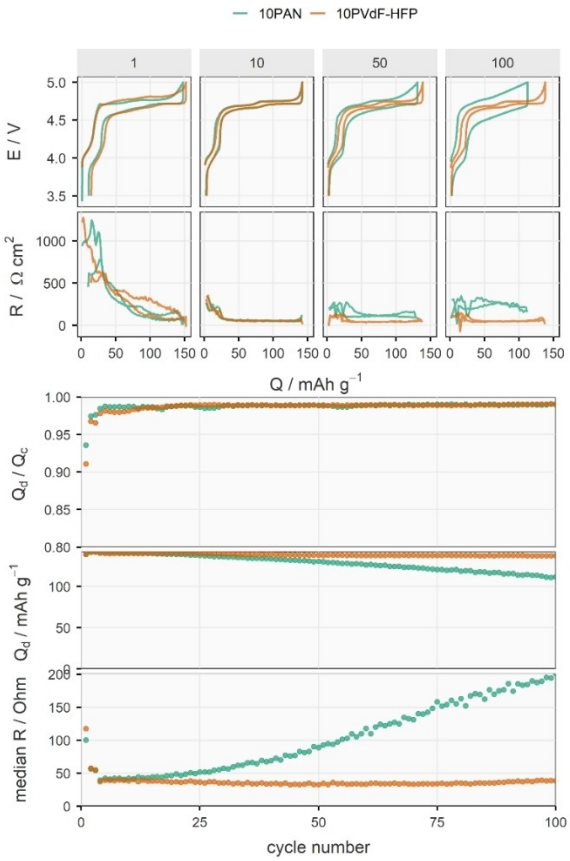

Figure 3. ICI data for LNMO half-cells with 10PAN and 10PVdF-HFP cells. In the 1st and 2nd rows, the voltage profiles and corresponding internal resistance changes against specific capacity in cycles 1, 10, 50, and 100 are displayed. Coulombic efficiency, discharge capacity and median resistance changes over 100 cycles are shown in the 3rd, 4th and 5th row of the figure.

resistance is one of the major causes for the rapid capacity fade. The sloping voltage profile and the lack of a sharp end point at the end of charge of the 100th cycle in the PAN cell suggest that there is a significant *iR* drop in the electrode and that resistance limits charging. Another interesting observation is that the lower plateau discharge capacity seems to be more or less similar, indicating that there is no significant loss of active material. The high internal resistance causes the voltage of the cell to drop, and the cell is thereby prompted to an early shut down before full capacity is reached. The high resistance can also correspond to a poor electronic wiring of the electrode, caused by decomposition products, which render some part of the electrode inaccessible for intercalation reactions and thereby leads to a low capacity.

Since the ICI technique only provides information on the overall cell resistance, electrochemical impedance spectroscopy (EIS) measurements were performed to better understand the origin of resistance evolution in the PAN-based cells. After every 10 galvanostatic cycles, the impedance of the 20PAN cell was measured at 4.6 V. The equivalent circuit used to fit the experimental data is provided in Figure 4. The equivalent circuit comprises two parallel resistor-constant phase element (R-CPE or RQ) circuits (R_2Q_1 and R_3Q_2) in series with each other and in

Research Article
doi.org/10.1002/batt.202200279
Chemistry Europe
European Chemical Societies Publishing

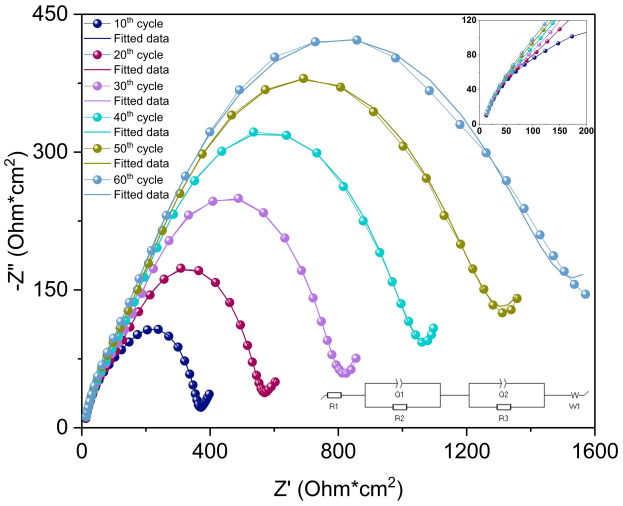

Figure 4. Electrochemical impedance spectra of 20PAN cell.

series with a resistor R_1 and Warburg element W_1. R_1 represents the frequency-independent resistance arising from the ionic resistance in the electrolyte as well as the electronic resistance in the electrodes, current collectors and cables; W_1 represents mass transport in the cell at low frequency. R_2Q_1 and R_3Q_2 represent two distinct time constants in the middle-to-low frequencies which are expected to correspond to processes associated with both porous electrodes, including contact resistance, SEI film resistance and charge transfer resistance, each in parallel with capacitive processes. The observation of increase in diameter of both the semi-circles (i.e., R_2 and R_3) with cycle number as observed in Figure 4 supports the evolution of an interfacial resistance in the positive electrode with cycling, even though it is in practice not possible to distinguish between the resistances arising from SEI/contact resistance and charge transfer resistances with this experimental setup. During the first EIS measurement, as derived from the fitted data, R_2 appears to be ~123.4 $\Omega\,cm^2$, which rises up to ~125.3 $\Omega\,cm^2$ during the second measurement, while R_3 rises from ~230.8 $\Omega\,cm^2$ to ~420 $\Omega\,cm^2$. It can be noted that the resistance increase is dominated by only one major but undefined process, R_3. This means that it is less likely that it is two separate processes increasing at the same time (e.g., resistance at both the electrodes going up simultaneously, or both contact resistance and SEI resistance increasing at the same time). It can be noticed that this resistance, R_3, increases substantially with each measurement, showing that the cell resistance increase is indeed correlated to surface effects in the electrodes, as opposed to other processes such as decomposition in the bulk electrolyte. Given that no similar increase in resistance is observed in the electrode with PVdF-HFP binder, this suggests a resistance within the electrode arising from PAN degradation.

Synthetic charge-discharge profile voltammetry

The first cycle Coulombic efficiency in the PAN-based cells decreases with increasing amount of binder in the PAN-based cells, as observed in the galvanostatic cycling results in Figure 2(b). This indicates a degradation or decomposition reaction, different from the cell with PVdF-HFP. In order to confirm this, synthetic charge-discharge voltammetry technique was utilized.[28] The LNMO charge and discharge voltage profiles has been divided into two regions, namely, the lower plateau region (< 4.3 V vs. Li/Li^+) and the upper plateau region (> 4.3 V vs. Li/Li^+) as shown in Figure 5(a). The SCPV technique is intended to provide an indicator of parasitic charge, i.e., charges arising from side reactions such as electrolyte or binder degradation, passed during each region and in each cycle. Electrodes with glassy carbon, replacing the LNMO active material, were prepared for this study. Glassy carbon with similar particle size as that of LNMO was chosen in order to mimic a porous electrode with a surface area comparable to that of the LNMO electrode. For the SCPV measurements, the electrode composition was chosen to match the electrode density of the LNMO electrodes used in the galvanostatic cycling tests. A set of cells with glassy carbon electrodes that contained either 20 volume percent of PAN or PVdF-HFP binder were studied using this technique. Both electrolyte and binder decomposition can account for the amount of charge formed during each cycle. The changes in amount of charge in each cell are expected to originate from differences in the binder concentration and further degradation of it, since the electrolyte was LP40 in all cases and with similar quantities.

The 20 vol% PAN and 20 vol% PVdF-HFP in Figure 5(b and c), respectively, demonstrate that a higher amount of charge is passed for the 20 vol% PAN-based glassy carbon cell in the anodic sweep of the first cycle. The higher amount of charge in the anodic sweep in the first cycle indicates oxidation or decomposition of both the electrolyte and the binder in each case. These tests thus confirm more extensive decomposition reactions for the PAN-based samples, although the technique cannot distinguish between electrolyte and binder decomposition.

On-line electrochemical mass spectrometry

In order to better understand the mechanism of the degradation reactions and to identify the major overall gaseous decomposition products in the PAN-based cell, the electrode with the highest concentration, i.e., 20PAN, was chosen for the OEMS experiments. The results were also compared with a corresponding PVdF-HFP cell. The LNMO electrodes were cycled both against delithiated LFP and lithium metal using LP40 electrolyte after an OCV rest period of 5.7 hours (345 min).

Figure 6(a and b) shows the gas evolution rate in nmol/min plotted against the cell potential for 20PAN and 20PVdF-HFP half-cells. The first and second rows reflect the gassing from the first and second cycles respectively – gassing from the first cycle can arise from impurities on the electrode surface, and so

Research Article
doi.org/10.1002/batt.202200279

Chemistry Europe
European Chemical Societies Publishing

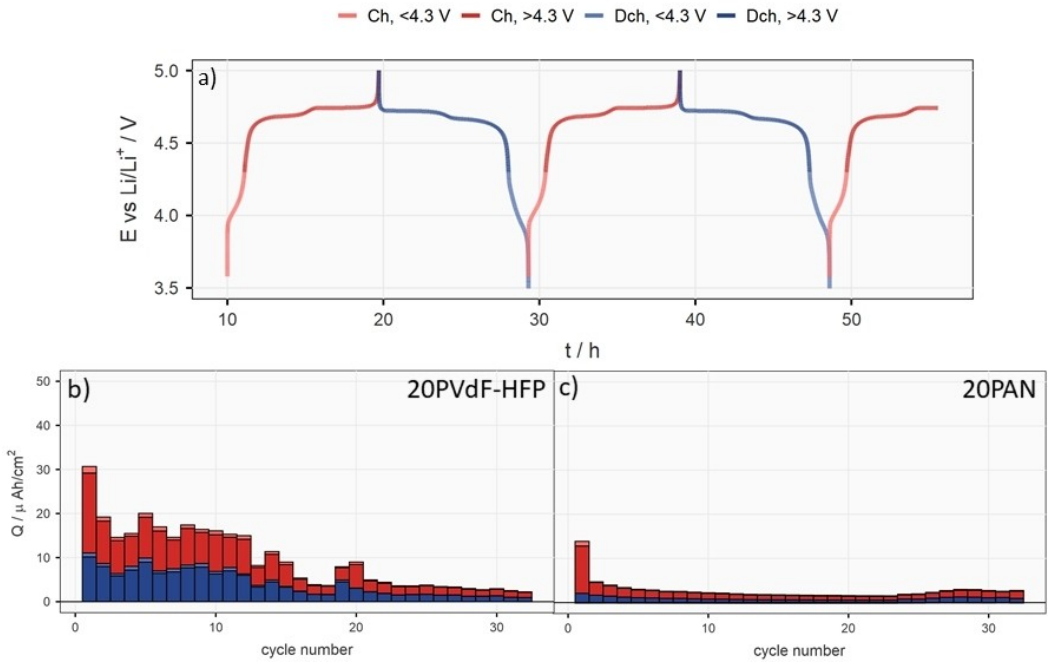

Figure 5. a) LNMO voltage profile divided into different regions such as a lower plateau region (< 4.3 V) and a higher plateau region (> 4.3 V) in both charge and discharge profiles; b) and c) show the amount of charge passed in each region with cycle number for glassy carbon electrodes with volume percent of 20PAN (4.58 mg) and 20PVdF-HFP (4.00 mg), respectively. The numbers in brackets show the amount of glassy carbon in the electrode.

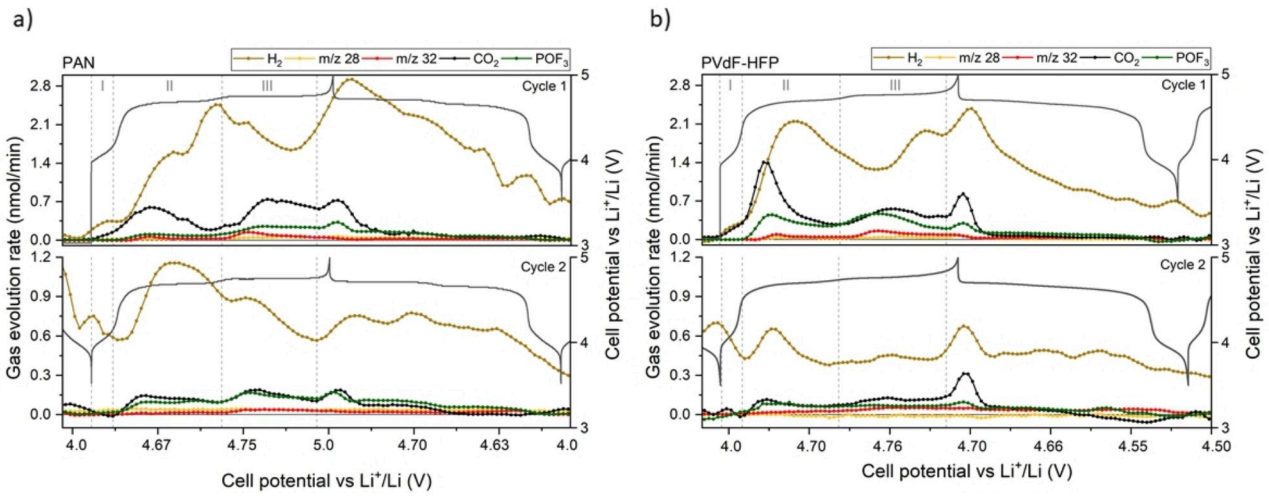

Figure 6. Gas evolution rate against cell potential vs. Li^+/Li for half cells using LNMO working electrodes containing (a) 20PAN and (b) 20PVdF-HFP binders. The first two cycles are shown separately in rows one and two respectively, both depicting H_2, CO_2, and POF_3 gasses and m/z values for 28 and 32. The three main plateaus of LNMO labelled I, II, and III are highlighted with dotted grey lines.

cannot always be attributed to relevant chemical and electrochemical processes. Each graph is divided into three regions: region I, Mn^{3+} to Mn^{4+}; region II, Ni^{2+} to Ni^{3+}; and region II, Ni^{3+} to Ni^{4+} corresponding to the three main redox steps of LNMO. A selection of 14 mass channels were chosen, namely m/z 2, 15, 16, 17, 18, 26, 27, 28, 32, 44, 52, 85 and 91, to monitor any potential volatile degradation products. Only 5 of the chosen 14 mass channels were able to detect some form of gassing. Of most interest were the nitrogen and cyano-containing products (channels *m/z* 27, 28 and 52) whose appearance would definitively indicate some form of PAN degradation. However, only channel *m/z* 28 showed a response, possibly originating from N_2 gas evolution, which is an unlikely byproduct in such a system, and more likely originating from CO which is identified in the same mass channel. Furthermore, it is only present in the full cell (Figure S3), and thus suggesting anodically activated processes that are not linked with the binder, but rather with typical electrolyte decomposition. A clear signal was also detected on channel *m/z* 32, which is most often associated with O_2 evolution, but other fragments

are observed here as well. No significant difference in *m/z* 32 is observed comparing the two binders, and no further conclusions are therefore drawn.

The remaining 3 channels that initiated a response on the mass spectrometer are identified as H_2 (*m/z* 2), CO_2 (*m/z* 44) and POF_3 (*m/z* 85). Both CO_2 and POF_3 form via potential-dependent processes. This is evidenced by the increase in both gasses at the border of each region during the charging step, i.e., when the potential increases. However, during the discharge step, there is significantly less gassing in all *m/z* channels for both systems apart from hydrogen which is likely formed as a result of the presence of lithium and not cathode or the binder. The relatively small overpotentials observed would not have such a large impact on the gassing. This discrepancy can be explained by the fact that during the charging step, exposed oxygens on the surface of the LNMO are able to interact with the electrolyte, contributing to oxidation reactions, whereas during the discharge step, the LNMO surface is now lithiated and unable to participate in any oxidative processes. After 2 cycles the 20PAN and 20PVdF-HFP cells produce a total amount of 380 nmol and 401 nmol of CO_2 respectively, which considering error margins are almost identical. The same is true for the amount of POF_3 produced (208 nmol and 257 nmol). This shows that these potential-activated processes are not influenced by the binder. Furthermore, it is important to note that the total amount of gas produced in both the systems under study is relatively small compared to what is expected from layered oxides in the same voltage regime. For example, ~55 nmol of CO_2 is released over both cycles for the 20PAN and 20PVdF-HFP cells, whereas a typical amount released from NMC811 half-cells is ~100,000 nmol; a value of 5 orders of magnitude larger.[29] Other layered oxides tend to release reactive oxygen at higher voltages that reacts with the electrolyte forming CO_2, whereas LNMO releases almost no oxygen.

In contrast to the potential-activated processes forming CO_2 and POF_3, H_2 evolution in both systems occurs independently of the potential and continues to evolve during the discharge step. Onset times for the H_2 evolution in both systems tends to occur just after other gasses have formed, suggesting a chemically driven autocatalytic process. By integrating the curves, we can see that the 20PAN cell produces more H_2 (or protons) than the 20PVdF-HFP cell, with 2444 nmol versus 1916 nmol after 2 cycles, respectively. This difference suggests that the presence of PAN in the electrode is promoting a part of the autocatalytic proton production – and is perhaps a cause for future cell deterioration with further cycling.[30,31]

X-ray photoelectron spectroscopy

XPS studies were conducted on a pristine 20PAN electrode and a 20PAN electrode that had been cycled for 100 cycles to investigate the degradation products formed on the surface of the electrode after cycling. The data obtained from these experiments are presented in Figure 7. The C 1s spectrum of the pristine electrode, with no contact to electrolyte is shown in Figure 7(a). The C 1s spectrum of the pristine electrode exhibits a peak at 284.8 eV, which is attributed to the carbon black, and all spectra were calibrated with respect to this peak. A relatively lower intensity peak at a lower binding energy, 283.1 eV, is assigned to C=C, which is also associated with the graphitic regions of carbon black. Two different peaks at 285.3 eV and 287.4 eV, respectively, are assigned to adsorbed species such as C–O and C=O. The peak at 285.9 eV corresponds to C≡N, originating from the PAN binder. Figure 7(b) shows the N1s spectrum of the pristine electrode, which exhibits a single peak at 399 eV arising from the nitrile group in the binder. On the other hand, the N 1s spectrum of the cycled electrode in Figure 7(d) indicates two distinct nitrogen environments. This clearly demonstrates that the PAN binder has undergone a degradation process. The peak corresponding to the binding energy value 399.2 eV indicates the presence of sp-hybridised (C≡N) and the broad peak at 399.8 eV suggests the presence of sp^2-hybridised (C=N) nitrogen environment or other nitrogen-containing compounds. At 286.2 and 286.6 eV, respectively, the C 1s spectrum in Figure 7(c) verifies the presence of both C≡N and C=N. A plausible reaction, based on the above findings and data in the literature, would be the decomposition of PAN to form nitrogen-containing compounds.[32,33] These could be formed as a result of intramolecular cyclization, as has previously been proposed by Aggour and Aziz[34] at other chemical conditions, but could also be possible at the high operating voltages of LNMO. A potential decomposition reaction that could occur when radical and/or cationic species are formed in the highly oxidising environment during the charging step of the LNMO cell would result in cyclization of PAN, as suggested in the schematic in Figure 8. The cyclized products may thereafter undergo further chemical changes. Taking the XPS and OEMS result together, they show that the degradation products generated during electrochemical cycling in the LNMO electrode remain in the electrode and do not form volatile species to any significant degree.

Solubility test

To determine the solubility of the PAN binder in the solvent mixture of EC and DEC, as well as the individual solvents in the electrolyte, a simple solubility test was performed. Figure 9 depicts the outcomes of these tests. It could be observed that PAN is completely soluble in the EC solvent (EC was melted at 40 °C before adding PAN) but insoluble in DEC. The solute formed a precipitate and the solvent appeared cloudy when PAN was added to the EC:DEC solvent combination. This means that PAN – in contrast to PVdF-HFP – swells in the EC:DEC solvent mixture, which is likely influencing the cell behaviour. Swellability of the binder usually results in a loss of adhesion between the active particles and the current collector, as well as a loss of cohesion between the active particles, consequently resulting in the loss of electrode integrity. ^{13}C nuclear magnetic resonance spectroscopy (NMR) experiments were performed on the electrolyte extracted from a cycled 20PAN cell to inves-

Research Article
doi.org/10.1002/batt.202200279
Chemistry Europe
European Chemical Societies Publishing

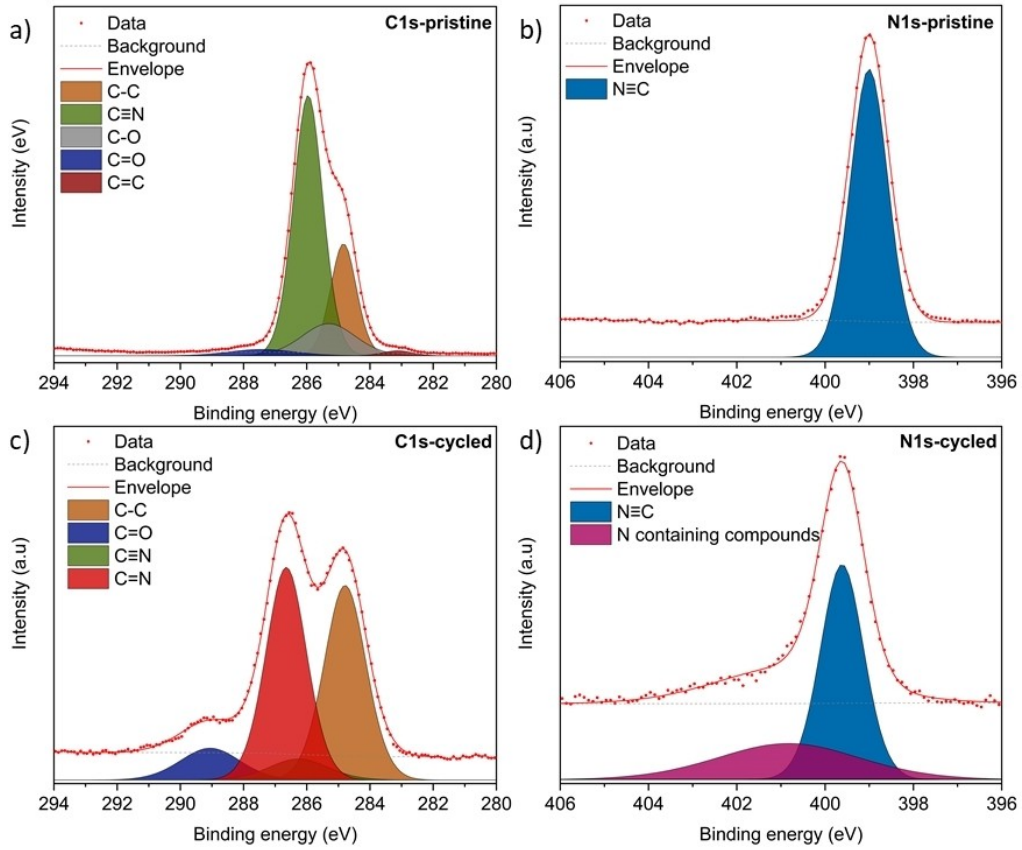

Figure 7. Deconvolution spectra of pristine 20PAN electrode a) C 1s, b) N 1s and cycled 20PAN electrode c) C 1s and d) N 1s.

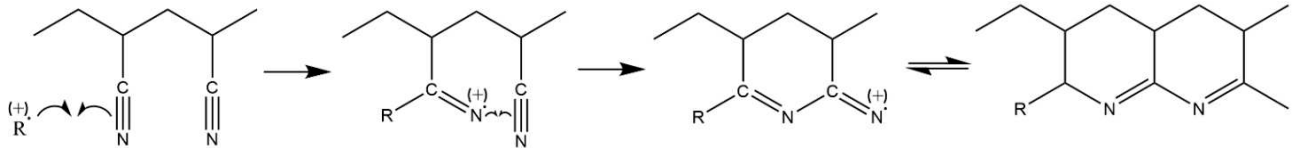

Figure 8. Schematic representation of the proposed decomposition of PAN.

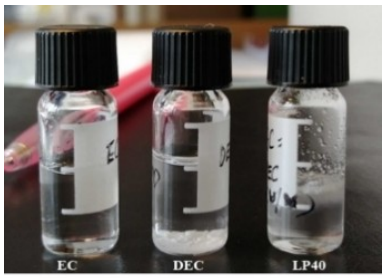

Figure 9. Solubility tests using PAN mixed with EC, DEC and LP40 solution.

tigate if there is any dissolution of PAN into the electrolyte. However, no indication of the nitrile group, which is expected in the 110–120 ppm region, or the –C=N– group, which is expected in the 145–150 ppm region, was found in the NMR measurements (see Figure S4), implying that the binder or degradation products from the binder have not dissolved in these cells.

PAN has been employed as a binder in negative electrodes such as graphite, $Li_4Ti_5O_{12}$ (LTO), silicon/graphite and silicon electrodes for LIBs previously,[17,35] but has so far not been employed as a cathode binder. Nevertheless, PAN has been targeted as a potentially useful high-voltage cathode binder due to its strong oxidative stability. The results presented here, however, suggest that it functions poorly as a binder in LNMO high-voltage cells, and that the stability can be put in question. If PAN is indeed oxidatively stable in general terms, it still obviously undergoes different types of reactions in the LNMO-based cell environments employed here – if not due to the high voltage, then due to other phenomena causing side-reactions, e.g., catalysis by the LNMO active material itself. The polymer used as an electrode binder is meant to serve many purposes, which include holding the active material together, assisting in the adherence of the electrode slurry to the current

collector, remaining chemically and electrochemically stable throughout the electrochemical processes occurring in the cell, and assisting in the formation of a stable passivation layer. Binder degradation creates a highly resistive layer and would also result in the loss of the ability to hold the active material together and the adhesion between the active material and the current collector. As a result, when a binder degrades, it loses its ability to facilitate good battery performance during cycling, and thereby causing capacity fade. Based on the above electrochemical and XPS results, it can be concluded that PAN causes high resistance and fast capacity decay in LNMO cells when utilised as a binder. It is understood that PAN decomposes at high voltages and is believed to undergo chemical changes as a consequence of intramolecular cyclization, resulting in other nitrogen-containing compounds.

In the various attempts where nitrile-based polymers have been used with LNMO or other high-voltage electrodes, it is not the PAN homopolymer that has been used, which renders a direct comparison less meaningful. However, the seemingly successful results shown for these nitrile-based systems also needs to be properly scrutinized. For example, the positive results in previous studies have occasionally been reported with a weak control experiment, such as a fast capacity decay in a cell with conventional PVdF binder in a short span of cycles, or without relevant and critical experimental details such as electrode loadings. Moreover, considering the results of the solubility tests presented here, the solubility of PAN in EC-based electrolytes must also be taken into account for further studies.

Another interesting observation is that binders with significantly lower theoretical oxidative stability than PAN, such as carboxymethyl cellulose (CMC), has been shown to function as equally well as PVdF-HFP binders in several battery cathode chemistries, including LNMO.[36–39] The probable reason for the good performance of binders such as CMC could be that any decomposition products formed during cell cycling form a stable passivating layer on the cathode, allowing for stable cycling. This implies that kinetic stability, rather than thermodynamic stability, is the deciding factor in a practical high-voltage cell.

Conclusion

Nitriles are generally understood to offer high oxidation stabilities, with stabilities often stated to be in excess of the operating potential of the LNMO cathode. Following the known successful approach of binder selection to improve surface stability on graphite anodes, we here applied PAN as a binder for LNMO and found that while PAN coats the electrode well, the corresponding cells display increasing capacity fade with a higher binder concentration, contrary to this initial hypothesis. Electrochemical analysis and ICI reveal an increasing resistance and additional parasitic reactions attributable to the degradation of PAN. The presence of a second nitrogen environment in the 20PAN cycled electrode was discovered by XPS, showing that PAN does decompose. This raise concerns over using polynitriles in high-voltage battery cells. On the other hand, other binders such as CMC, sodium alginate, etc., with reportedly lower electrochemical stability have recently shown to offer similar performance as that of PVdF in spite of their expectedly lower resistance to oxidation.[40] This indicates that the electrochemical stability of the binder is not always the most crucial point for successful functionality in the battery electrode. Taken together, these results should encourage further research into the factors governing materials compatibility at the electrode interfaces, and more careful analysis of material degradation.

Experimental Section

Materials: LNMO powder (TBM-129, average diameter of 5–20 μm, Haldor Topsoe A/S), polyacrylonitrile (PAN, $M_w = 150{,}000$, Sigma Aldrich), N-methylpyrrolidone (NMP, Sigma Aldrich), poly(vinylidene difluoride-hexafluoropropylene) (PVdF-HFP, Kynar FLEX 2801, Arkema), super P C65 (Imerys), carbon-coated aluminium foil (20 μm thick, SDX, Showa Denko) and coin cell parts (CR2025, Ni-plated, Hohsen) were used as received. Microporous monolayer polypropylene Celgard 2500 separators were cut (16 mm diameter) and dried at 70 °C for 5 h under vacuum. Li metal foil (125 μm, Cyprus Foote Mineral) was used as received but stored under argon atmosphere. 1 M $LiPF_6$ in 1:1 ethylene carbonate:diethyl carbonate (EC:DEC, LP40, Gotion) electrolyte was used as received and stored under argon.

Electrode preparation and cell assembly: Binder solutions were prepared with PAN in NMP and PVdF-HFP in the same solvent. Electrode slurries were prepared with LNMO active material, varying amounts of PAN and PVdF-HFP binder concentrations (2.5 wt.%, 5 wt.%, 10 wt.%, 15 wt.%, and 20 wt.%) and a fixed concentration of 5 wt.% carbon black (C-ENERGY Super C65, Imerys. For convenience, 2.5 wt.% PAN, 5 wt.% PAN, 2.5 wt.% PVdF-HFP and so on are defined as 2.5PAN, 5PAN, 2.5PVdF-HFP, respectively, in the following. The slurries were mixed using a shaker ball mill for 30 min at 25 rpm and were cast on carbon-coated aluminium foil using a laboratory doctor blade with a wet film thickness of 150 μm. The electrodes had an active mass loading of 3.0–4.5 mg cm^{-2}. The electrodes were dried at 70 °C for 12 h and were cut into 13 mm discs, pressed at 3 tons for 3 min and were further dried at 120 °C under vacuum in an Argon filled glove box.

All the electrodes were tested in half cells against lithium metal in coin cells. 80 μL ofLP40 was used as an electrolyte. Lithium foil with diameter 15 mm were used as a counter electrode. Two Celgard separators were placed in between the working and counter electrode. Electrolyte was added and soaked the separators prior to placing the lithium metal foil in the cell.

Surface characterization: A Zeiss 1550 field emission secondary electron microscope (FE-SEM) equipped with an energy dispersive X-ray (EDX) detector was used to observe the surface morphology of the electrodes. Secondary electron microscope (SEM) images and EDX maps were obtained at an accelerating voltage of 5 kV to reduce the charging effects and binder decomposition on the electrode surfaces. The working distance was maintained at 5 mm for all the measurements.

Electrochemical characterization:

Galvanostatic cycling: The half-cells were galvanostatically cycled on an ArbinBT-2043 cycling equipment at C/10 rate for 3 cycles and C/5 rate for the remainder of the cycles after a rest time of 10 h at open circuit voltage (OCV) conditions. The cells were cycled at room temperature and between the voltage limits of 3.5 V to 5.0 V; all the voltage or potential values refer to the reference Li/Li^+ redox couple. The specific current of 147 $mA\,g^{-1}$ corresponds to a charge-discharge rate of 1 C.

Intermittent current interruption and electrochemical impedance spectroscopy: Half-cells with LNMO electrodes containing 10 wt.% PAN (active mass loading: 4 $mg\,cm^{-2}$) and PVdF-HFP (active mass loading: 2.88 $mg\,cm^{-2}$) binder were cycled on an Arbin BT-2043 equipment at C/10 rate after an OCV period of 10 h at room temperature. Every 5 min, 1 s of current interruptions were made, and the voltage responses were recorded at 0.1 s. The analysis procedure was done as according to the routine developed by M. J. Lacey.[41]

LNMO half-cell containing 20PAN electrode, in a two-electrode set-up was cycled in a Biologic MPG2 equipped with a galvanostat and potentiostat channel at C/10 rate after an OCV period of 10 hours. After every 10 cycles, the cell was held at 4.6 V for 15 minutes, and the impedance spectrum was obtained in the potential controlled mode with a peak-to-peak amplitude of 10 mV in the 20 kHz to 100 mHz frequency range.

Synthetic charge-discharge profile voltammetry: Glassy carbon (GC) (2–12 μm) electrodes with carbon black (CB) and PAN binder were prepared. A set of electrodes with 75:20:5 volume percent of GC:PAN:CB and GC:PVdF-HFP:CB were made. It should be noted that the fraction of electrode components is in volume fraction instead of mass fraction. Synthetic charge-discharge profile voltammetry (SCPV)[28] was performed on a VMP2 potentiostat (BioLogic) at room temperature. The charge-discharge voltage profiles used in the SCPV technique were obtained from an LNMO | LP40 | Li cell cycled between 3.5 and 5 V vs. Li/Li^+ from an Arbin BT cycler at room temperature. The glassy carbon electrode with 20 vol% PAN binder was cycled in a half-cell with 80 μL LP40 electrolyte using the LNMO charge-discharge profiles. Comparisons were made a with cell containing electrode with PVdF-HFP binder at the same concentration.

On-line electrochemical mass spectrometry: Gas analysis was carried out using an OEMS setup designed and validated by Lundström et al.[42] Two separate LNMO electrodes with 20 wt.% PAN and PVdF-HFP binder were coated on a stainless steel mesh with active mass loadings 4.9 $mg\,cm^{-2}$ and 5.0 $mg\,cm^{-2}$, respectively. Each electrode was then separately cycled at C/10 against LFP delithiated to a 10% lithiation degree. The OEMS cell was assembled with LFP on the bottom followed by two 2500 Celgard separators in 200 μL LP40 electrolyte (Solvionics), the LNMO working electrode, a stainless steel current collector, and a spring. Once assembled, the cell was placed in an oven set to 30 °C and connected with the mass spectrometer (QME220, Pfeiffer). Gas was sampled from the cell every 10 min while continuously measuring the total pressure. The mass spectrometer was set to continuously analyse 14 different *m/z* channels and the electrochemistry was controlled by a potentiostat (Astrol Bat-Small, Switzerland).

X-ray photoelectron spectroscopy: The XPS experiments were performed on pristine and cycled 20PAN LNMO electrodes in a Kratos Axis Supra+ X-ray photoelectron spectrometer with an Al K (1486.6 eV) X-ray source. The 20PAN cycled electrode was dissembled from the cell and was rinsed with dimethyl carbonate (DMC) and dried further to remove any residual electrolyte. To avoid any air contact, the XPS sample was prepared inside the glovebox and the sample holder was vacuum-sealed before being moved into the measurement chamber. The data was analysed with CasaXPS software and with the hydrocarbon peak energy corrected to 284.8 eV. The entire spectrum was calibrated versus the hydrocarbon peak and is presented without any normalization.

Nuclear magnetic resonance spectroscopy: The cycled electrolyte was extracted from the cell and characterized by ^{13}C NMR spectroscopy to identify any binder components dissolved in the electrolyte during cell cycling. N,N-Dimethyl-formamide-d_7 (DMF) was used as the solvent. The chemical shifts were measured in parts per million using a 300 MHz Bruker spectrometer.

Acknowledgements

We thank our colleagues at Volkswagen AG, Germany, for fruitful discussions on this paper, especially Dr. Junli Shi. We thank Haldor Topsoe A/S, Denmark, for providing the LNMO material and for fruitful discussions with Dr. Jonathan Højberg and Dr. Christian Fink Elkjaer. Dr. Guiomar Hernández is acknowledged for guidance in SEM measurements. Dr. Andrew Naylor and Ignacio Andrés Cuevas Zuviría are acknowledged for helpful XPS discussions. The impartial financial support provided by Volkswagen AG and Scania CV AB is gratefully acknowledged. The STandUp for Energy consortium is acknowledged for the support. E.J.B. acknowledges Knut and Alice Wallenberg (KAW) Foundation (Grant 2017.0204) and Stiftelsen för Strategisk Forskning (SSF, FFL18-0269) for financial support. We acknowledge Myfab Uppsala for providing facilities and experimental support. Myfab is funded by the Swedish Research Council as a national research infrastructure.

Conflict of Interest

The authors declare no conflict of interest.

Data Availability Statement

The data that support the findings of this study are available from the corresponding author upon reasonable request.

Keywords: LNMO · high-voltage cathode · binder · lithium-ion battery · oxidative decomposition

[1] B. Aktekin, M. J. Lacey, T. Nordh, R. Younesi, C. Tengstedt, W. Zipprich, D. Brandell, K. Edström, *J. Phys. Chem. C* **2018**, *122*, 11234–11248.
[2] B. Aktekin, R. Younesi, W. Zipprich, C. Tengstedt, D. Brandell, K. Edström, *J. Electrochem. Soc.* **2017**, *164*, A942–A948.
[3] J. B. Goodenough, Y. Kim, *Chem. Mater.* **2010**, *22*, 587–603.
[4] J.-H. Kim, N. P. W. Pieczonka, L. Yang, *ChemPhysChem* **2014**, *15*, 1940–1954.
[5] B. Aktekin, F. Massel, M. Ahmadi, M. Valvo, M. Hahlin, W. Zipprich, F. Marzano, L. Duda, R. Younesi, K. Edström, D. Brandell, *ACS Appl. Mater. Interfaces* **2020**, *3*, 6001–6013.
[6] M. Kunduraci, G. G. Amatucci, *Electrochim. Acta* **2008**, *53*, 4193–4199.
[7] L. Wan, Y. Deng, C. Yang, H. Xu, X. Qin, G. Chen, *RSC Adv.* **2015**, *5*, 25988–25997.

[8] T.-F. Yi, Y. Xie, M.-F. Ye, L.-J. Jiang, R.-S. Zhu, Y.-R. Zhu, *Ionics* **2011**, *17*, 383–389.
[9] J. W. Kim, D. H. Kim, D. Y. Oh, H. Lee, J. H. Kim, J. H. Lee, Y. S. Jung, *J. Power Sources* **2015**, *274*, 1254–1262.
[10] D. Kim, S. Uchida, H. Shiiba, N. Zettsu, K. Teshima, *Sci. Rep.* **2018**, *8*, 11771.
[11] J.-H. Cho, J.-H. Park, M.-H. Lee, H.-K. Song, S.-Y. Lee, *Energy Environ. Sci.* **2012**, *5*, 7124–7131.
[12] J. Alvarado, M. A. Schroeder, M. Zhang, O. Borodin, E. Gobrogge, M. Olguin, M. S. Ding, M. Gobet, S. Greenbaum, Y. S. Meng, K. Xu, *Mater. Today* **2018**, *21*, 341–353.
[13] M. Y. Abeywardana, N. Laszczynski, M. Kuenzel, D. Bresser, S. Passerini, B. Lucht, *Int. J. Electrochem.* **2019**, *2019*, 8636540.
[14] F. Jeschull, M. J. Lacey, D. Brandell, *Electrochim. Acta* **2015**, *175*, 141–150.
[15] J.-T. Li, Z.-Y. Wu, Y.-Q. Lu, Y. Zhou, Q.-S. Huang, L. Huang, S.-G. Sun, *Adv. Energy Mater.* **2017**, *7*, 1701185.
[16] J. Liang, D. Chen, K. Adair, Q. Sun, N. G. Holmes, Y. Zhao, Y. Sun, J. Luo, R. Li, L. Zhang, S. Zhao, S. Lu, H. Huang, X. Zhang, C. V. Singh, X. Sun, *Adv. Energy Mater.* **2021**, *11*, 2002455.
[17] L. Gong, M. H. T. Nguyen, E.-S. Oh, *Electrochem. Commun.* **2013**, *29*, 45–47.
[18] P. Hu, J. Chai, Y. Duan, Z. Liu, G. Cui, L. Chen, *J. Mater. Chem. A* **2016**, *4*, 10070–10083.
[19] J. Mindemark, M. J. Lacey, T. Bowden, D. Brandell, *Prog. Polym. Sci.* **2018**, *81*, 114–143.
[20] Y. Abu-Lebdeh, I. Davidson, *J. Electrochem. Soc.* **2009**, *156*, A60.
[21] S. Panero, D. Satolli, A. D'Epifano, B. Scrosati, *J. Electrochem. Soc.* **2002**, *149*, A414–A417.
[22] W. Lin, *Int. J. Electrochem. Sci.* **2017**, 12047–12059.
[23] S. Tanaka, T. Narutomi, S. Suzuki, A. Nakao, H. Oji, N. Yabuuchi, *J. Power Sources* **2017**, *358*, 121–127.
[24] H. Chen, M. Ling, L. Hencz, H. Y. Ling, G. Li, Z. Lin, G. Liu, S. Zhang, *Chem. Rev.* **2018**, *118*, 8936–8982.
[25] X. Wang, C. Xiao, H. Liu, M. Chen, J. Hao, Y. Wu, *RSC Adv.* **2018**, *8*, 27754–27762.
[26] Y. C. Chien, A. S. Menon, W. R. Brant, D. Brandell, M. J. Lacey, *J. Am. Chem. Soc.* **2020**, *142*, 1449–1456.
[27] A. R. Mandli, A. Kaushik, R. S. Patil, A. Naha, K. S. Hariharan, S. M. Kolake, S. Han, W. Choi, *Int. J. Energy Res.* **2019**, *43*, 2044–2056.
[28] A. Mathew, M. J. Lacey, D. Brandell, *J. Power Sources Adv.* **2021**, *11*, 100071.
[29] D. Streich, C. Erk, A. Guéguen, P. Müller, F.-F. Chesneau, E. J. Berg, *J. Phys. Chem. C* **2017**, *121*, 13481–13486.
[30] P. Arora, R. E. White, M. Doyle, *J. Electrochem. Soc.* **1998**, *145*, 3647–3667.
[31] C. L. Campion, W. Li, B. L. Lucht, *J. Electrochem. Soc.* **2005**, *152*, A2327.
[32] C. Bureau, G. Deniau, F. Valin, M.-J. Guittet, G. Lécayon, J. Delhalle, *Surf. Sci.* **1996**, *355*, 177–202.
[33] Y. Liu, X. Huang, J. Liu, J. Liang, X. Wang, *J. Mater. Sci.* **2020**, *55*, 4962–4969.
[34] Y. A. Aggour, M. S. Aziz, *Polym. Test.* **2000**, *19*, 261–267.
[35] L. Luo, Y. Xu, H. Zhang, X. Han, H. Dong, X. Xu, C. Chen, Y. Zhang, J. Lin, *ACS Appl. Mater. Interfaces* **2016**, *8*, 8154–8161.
[36] Z. Wang, N. Dupré, A.-C. Gaillot, B. Lestriez, J.-F. Martin, L. Daniel, S. Patoux, D. Guyomard, *Electrochim. Acta* **2012**, *62*, 77–83.
[37] M. Kuenzel, H. Choi, F. Wu, A. Kazzazi, P. Axmann, M. Wohlfahrt-Mehrens, D. Bresser, S. Passerini, *ChemSusChem* **2020**, *13*, 2650–2660.
[38] D. Bresser, D. Buchholz, A. Moretti, A. Varzi, S. Passerini, *Energy Environ. Sci.* **2018**, *11*, 3096–3127.
[39] G. D. Salian, J. Højberg, C. Fink Elkjær, Y. Tesfamhret, G. Hernández, M. J. Lacey, R. Younesi, *ChemistryOpen* **2022**, *11*, e202200065.
[40] W.-Y. Chou, Y.-C. Jin, J.-G. Duh, C.-Z. Lu, S.-C. Liao, *Appl. Surf. Sci.* **2015**, *355*, 1272–1278.
[41] M. J. Lacey, *ChemElectroChem* **2017**, *4*, 1997–2004.
[42] R. Lundström, E. J. Berg, *J. Power Sources* **2021**, *485*, 229347.

Manuscript received: June 22, 2022
Revised manuscript received: September 12, 2022
Accepted manuscript online: September 14, 2022
Version of record online: October 5, 2022